Available online at www.sciencedirect.com
ScienceDirect
Polymer 48 (2007) 2681–2691
polymer
www.elsevier.com/locate/polymer

Microstructure of Triton X-100/poly (ethylene glycol) complex investigated by fluorescence resonance energy transfer

Lingling Ge, Xiaohong Zhang, Rong Guo*

School of Chemistry and Chemical Engineering, Yangzhou University, Yangzhou 225002, PR China

Received 27 July 2006; received in revised form 23 January 2007; accepted 27 January 2007
Available online 1 February 2007

Abstract

The microstructure of Triton X-100 (TX-100)/poly (ethylene glycol) (PEG) complex has been investigated by fluorescence resonance energy transfer (FRET), dynamic light scatter (DLS), freeze-fractured transmission electron microscopy (FF-TEM) and ^{1}H NMR technology. The nonionic surfactant TX-100 and pyrene are employed as energy donor and acceptor respectively, and the average distance between them is calculated quantitatively in the systems of TX-100/PEG with different molecular weights (MW). The results of FRET study indicate that the presence of PEG leads to the separation of donor and acceptor in TX-100 micelle, suggesting that PEG chains insert into TX-100 micelles making the microstructure of PEG-bound TX-100 aggregates looser than that of free micelles, which is independent of the MW of PEG. However, FF-TEM, DLS and ^{1}H NMR studies show that the morphology of TX-100/PEG complex depends on the MW of the polymer: PEG with shorter chain (MW $<$ 2000 Da) insert into and wrap around TX-100 micelles and form sphere-like complex, while that with longer chain (MW $>$ 2000 Da) would interact with numbers of TX-100 micelles and form coral-shaped clusters. In addition, the effects of temperature and alcohol on the microstructure of TX-100/PEG complex are studied.

Keywords: Poly (ethylene glycol); Nonionic surfactant; Microstructure

1. Introduction

The interaction of surfactants with macromolecules has been extensively studied for the past 50 years. The protein/surfactant systems were first investigated because of their biological importance. However, with the appearance of well-defined synthetic polymers, the research of the interaction of surfactant with macromolecules has been extended to the polymer/surfactant interaction as the simultaneous presence of them is required to achieve ideal dispersion effects which are relevant to the manufacture of many products including detergents, cosmetics, paints and so on. So far, most of these studies [1–5] have been focused on nonionic polymers and ionic surfactants due to their simple structures and interactions, and the configuration of polymer/surfactant complex has been accepted as ''string of beads'' in which the polymer chain connects micelle-like surfactants by threading through them.

Systems of nonionic polymer/surfactant possess many properties superior to those of ionic ones like higher stability, better biologic compatibility and lower toxicity, and they have been widely used in material synthesis and biology simulation [6–11]. But the studies on the interactions of nonionic polymer/surfactant are rarely seen. Borisov and Halperin [12] used the concept of polysoap micelles to describe the effect of bridging interaction between surfactant and polymer, and suggested that the polymer segments may penetrate into the micelles. Qiao and Easteal [13] investigated the effect of polymer chain length and micelle size on the cloud point of TX-100$_{(aq)}$, and they proposed two possible models to describe the polymer–surfactant interactions. However, nonionic water soluble polymers can interact with surfactant aggregates in many ways: (1) hydrogen bond may drive polymer chains to

* Corresponding author. Fax: +86 514 7311374.
E-mail address: guorong@yzu.edu.cn (R. Guo).

0032-3861/$ - see front matter © 2007 Published by Elsevier Ltd.
doi:10.1016/j.polymer.2007.01.061

be absorbed on the shell of surfactant micelles; (2) some segments of polymer may penetrate into hydrophilic groups of surfactant aggregates driven also by hydrogen bond; (3) polymer chain may also thread through the hydrophobic core of micelle and form ''string of beads'' aggregates. However, present views on the interaction mechanism and models are controversial. In addition, the penetration of polymer segments into the micelles will change micelle size, which is critical in material synthesis and biology simulation, but it is quite hard to find the change.

Fluorescence resonance energy transfer involves the energy transferred from an initially excited donor (D) to an acceptor (A). It can be used to calculate the average distance between D and A quantitatively, so it is referred to as ''spectroscopic ruler'', and it is the critical technique to study the biomacromolecules like protein and nucleic acid. Schild [14] used this technique for the first time to investigate the interaction between polymer and surfactant. Since then, fluorescent dual-labeling [15–19] and micelle solubilization [20–22] have been the main techniques to induct energy donor and acceptor for the study of energy transfer by its sensitivity to distance to monitor the structure change of polymer/surfactant complex. However, the process of either fluorescent labeling or solubilization of fluorophores into surfactant aggregates may bring slight change of the microstructure of aggregates, which is a disturbance for structure monitoring. In this study, the surfactant TX-100 itself is employed as excitation energy donor, as it contains aromatic moiety, and trifle amount of pyrene is added as an energy acceptor in order to lessen the disturbance mentioned above. The energy transfer efficiency (E_T) from TX-100 to pyrene and the average distance (r) between phenyl rings of TX-100 and pyrene are calculated quantitatively to monitor the size change of the PEG-bond surfactant aggregates. Besides that, ^{1}H NMR technology is used to illustrate the mechanism of the interaction of the nonionic water soluble polymer PEG with TX-100, and dynamic light scatter is a useful technique to observe the form, size and distribution of aggregates in solution, what is more, freeze-fractured transmission microscopy provides us with eyes to ''see'' the various configurations of TX-100/PEG complexes with different polymer molecular weights.

2. Experimental section

2.1. Materials

Triton X-100 (TX-100, >99%, Sigma) was used as received. Pyrene (>99%) was obtained from Sigma and 6.33×10^{-4} mol/L pyrene stock solution was prepared in ethanol. Surfactant solutions with 0.76×10^{-6} mol/L pyrene were made by placing 5 μL of pyrene stock solution in a 5 mL test tube, evaporating the ethanol, adding appropriate surfactant solution, and sonicating for 15 min. Cetylpyridinium chloride (CPC, >99%) was purchased from Fluka. The investigated poly (ethylene glycols) (PEGs, MW = 400, 1000, 2000, 4000, 6000, 10,000, 20,000) were Aldrich products and the distribution of the MW agreed with a narrow Possion distribution. *n*-Propanol, *n*-butanol, *n*-pentanol, *n*-hexanol were purchased from Fluka. Doubly distilled water was used for all the experiments.

2.2. Fluorescence spectroscopy

All fluorescence measurements were taken on a Shimadzu RF-5301 (Japan) fluorescence spectrophotometer equipped with a thermostat (±0.5 °C). Solutions were equilibrated for at least 15 min before the measurement. TX-100 was excited at 285 nm and pyrene at 338 nm, and the ratio of the fluorescence intensity of the first (370 nm, I_1) to the third (381 nm, I_3) vibration bands of pyrene is used to probe the polarity of the microenvironment around pyrene [23].

2.3. UV–vis spectroscopy

The UV–vis absorption spectras were measured with a Shimadzu UV-2550 digital spectrophotometer (Japan). Absolute quantum yields (ϕ_f^D) were determined as in Ref. [24] using quinine bisulphate as a standard ($\phi_f = 0.55$).

2.4. ^{1}H NMR technology

^{1}H NMR experiments performed in this study were carried out with a Bruker AV-600 NMR spectrometer with a ^{1}H frequency of 600.13 MHz. One hundred and twenty eight times of accumulations were acquired generally. Water was used as solvent and D_2O (99.5%) was used as an external standard. Meanwhile, the presaturation method was used to further suppress the proton signal of the solvent.

2.5. Isothermal titration calorimetry (ITC)

ITC measurements were performed using a VP-ITC titration microcalorimeter (MicroCal Inc., Northampton, MA) at 25 ± 0.1 °C. The removable integrated injection-stirrer (250 μL) was filled with a concentrated surfactant aqueous solution (or surfactant solution in 5 wt% $PEG_{(aq)}$) which was titrated into the calorimeter vessel initially containing 1.438 mL of pure water (or 5 wt% $PEG_{(aq)}$) in the sample cell. Doubly distilled water was filled in the reference cell. The surfactant was titrated into the sample cell in multiple steps (5–10 μL) at the constant stirring speed of 502 rpm to ensure thorough mixing. The duration of each injection was 10 s and the time delay (to allow equilibration) between successive injections was 240 s. Raw data were obtained as a plot of heating rate (μcal s^{-1}) against time (min). These raw data were then integrated to obtain a plot of observed enthalpy change per mole of injected TX-100 (ΔH_{obs}, kJ mol^{-1}) against TX-100 concentration (mM). All experiments were repeated twice and the reproducibility was within ±2%.

2.6. Dynamic light scatter (DLS)

Measurements were carried out at a scattering angle of 90° using an ALV 5022 laser light-scattering (LLS) instrument

equipped with a cylindrical He–Ne laser (model 1145p-3083; output power = 22 mW at $\lambda = 632.8$ nm) in combination with an ALV SP-86 digital correlator with a sampling time range of 25 ns–40 ms. The LLS cell is held in a thermostat index matching vat filled with purified dust-free toluene, with the temperature controlled with ±0.02 °C. All solutions were filtered through a Millipore filter with a 0.22 μm pore size and thermostated at 25 °C for at least 0.5 h. Experiment duration was 10 min and each experiment was repeated two or more times. The intensity–intensity time correlation function $G^{(2)}(t,q)$ in the self-beating mode was measured, where t is the decay time and q is scattering vector ($q = (4\pi n/\lambda_0)\sin(\theta/2)$). $G^{(2)}(t,q)$ can be related to the normalized first-order electric field time correlation function $|g^{(1)}(t,q)|$ via the Siegert relation as [25]

$$G^{(2)}(t,q) = A\left[1 + \beta\left|g^{(1)}(t,q)^2\right|\right] \tag{1}$$

Where A ($\equiv \langle I(0)\rangle^2$) is the measured baseline. For the broadly distributed relaxation spectrum, $|g^{(1)}(t,q)|$ is related to a characteristic relaxation time distribution $G(\tau)$ as

$$\left|g^{(1)}(t,q)\right| \equiv \langle E(0,q)E^*(t,q)\rangle / \langle E(0,q)E^*(0,q)\rangle = \int_0^\infty G(\tau)\mathrm{e}^{-t/\tau}\,\mathrm{d}\tau \tag{2}$$

$G(\tau)$ can be calculated from the Laplace inversion of the measured $G^{(2)}(t,q)$ on the basis of Eqs. (1) and (2), and a translational diffusive coefficient distribution $G(D)$ by $\Gamma = Dq^2$, where $\Gamma = 1/\tau$, and the hydrodynamic radius distribution by the Stokes–Einstein equation: $R_h = k_B T/6\pi\eta D$, where η, k_B, and T are the solvent viscosity, the Boltzmann constant, and the absolute temperature, respectively. In this study, the CONTIN program supplied with the correlator was used.

2.7. Freeze-fractured transmission electron microscopy (FF-TEM)

For the preparation of replica, a small amount of sample was placed in a sample cell. Then the cell was swiftly plunged into liquid nitrogen, and then the frozen samples were fractured and replicated in a freeze-fractured apparatus (Balzers BAF 400D). Replicas were examined with transmission electron microscope (TEM, Tecnai 12 Philip, Holland).

The aggregated number of TX-100 micelle was obtained as in Ref. [26].

The temperature for this experiment was kept at 25 ± 0.1 °C.

3. Results and discussion

3.1. Energy transfer in TX-100 aqueous solution

Förster [27] proposes that resonance energy transfer occurs by a dipole–dipole long-range coupling interaction which depends on certain spectroscopic and geometric properties of the donor–acceptor pair. According to Förster theory, the efficiency of energy transfer depends mainly upon the following factors [28]: the extent of spectral overlap between the donor emission and acceptor absorption, the quantum yield of the donor (ϕ_f^D), the relative orientation of the donor and acceptor transition dipoles, and the distance between them. Fig. 1 shows emission spectrum for TX-100 and absorption spectrum for pyrene, and there is a large overlap zone. Besides that, TX-100 has a high value of ϕ_f^D (experimental value is 0.235). So TX-100/pyrene is an appropriate donor–acceptor pair for Förster energy transfer. It can be seen from Fig. 2 that the relative fluorescence intensity of TX-100 decreases with the addition of pyrene and that five emission peaks for pyrene [29] appear, indicating that part of the energy of excited state TX-100 molecules is transferred to ground state pyrene molecules and the emission spectrum of pyrene appears.

Förster theory shows that the energy transfer efficiency (E_T) is in inverse proportion to the sixth power of the distance (r) between the donor and acceptor [30]:

$$E_T = \frac{R_0^6}{R_0^6 + r^6} \tag{3}$$

$$E_T = 1 - \frac{F}{F_0} \tag{4}$$

Here E_T can be obtained by the relative fluorescence intensity of donor in the absence (F_0) and presence (F) of acceptor by Eq. (4), and R_0 is the Förster radius, i.e. the critical distance at which the decay rate of donor is equal to the energy transfer rate from donor to acceptor. R_0 is expressed as:

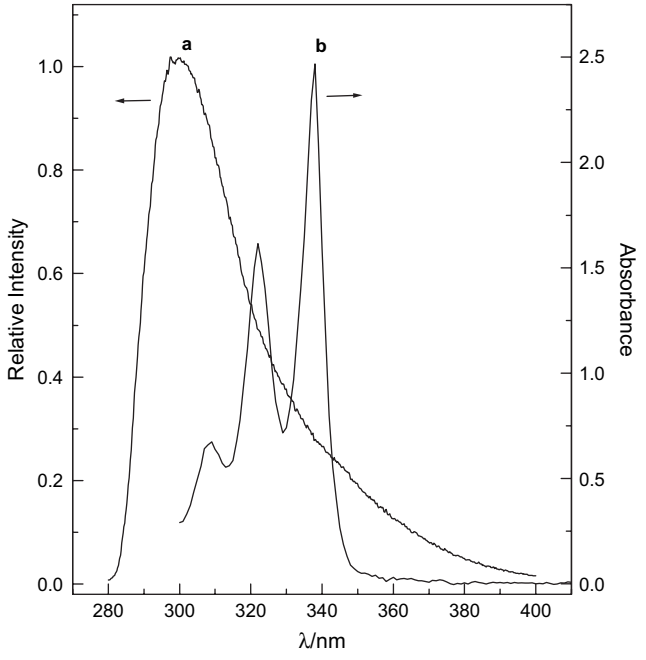

Fig. 1. Emission spectrum of TX-100$_{(aq)}$ (a) and absorption spectrum of pyrene in TX-100$_{(aq)}$ (b).

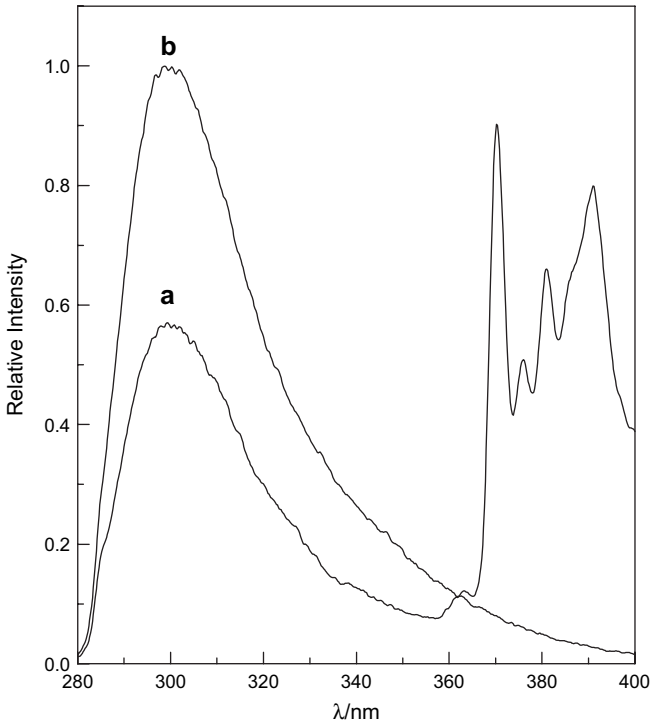

Fig. 2. Emission spectrum of TX-100 in the presence (a) and absence (b) of pyrene.

$$R_0^6 = \frac{9000\,(\ln 10)K^2\phi_f^{\mathrm{D}}}{128\pi^5 N n^4} J \quad \text{in } \mathring{\mathrm{A}}^6 \tag{5}$$

where k^2 is the factor expressing the relative orientation of donor and acceptor, and $k^2 = 2/3$ for random orientation as in fluid solution [30,31], n is refractive index of the medium, N is Avogadro number, ϕ_f^{D} is quantum yield of the donor in the absence of acceptor, and J is overlap integral expressed in units of $\mathrm{M}^{-1}\,\mathrm{cm}^3$, which is calculated by numerical integration:

$$J = \int_0^\infty F_{\mathrm{D}}(\lambda)\varepsilon_{\mathrm{A}}(\lambda)\lambda^4\,\mathrm{d}\lambda \tag{6}$$

Here $F_{\mathrm{D}}(\lambda)$ is corrected fluorescence intensity of the donor in the region of λ to $(\lambda + \Delta\lambda)$, with the total intensity normalized to unity, and $\varepsilon_{\mathrm{A}}(\lambda)$ is the extinction coefficient of the acceptor at λ in $\mathrm{M}^{-1}\,\mathrm{cm}^{-1}$.

Fig. 3A shows the effects of TX-100 concentration on its relative fluorescence intensity in the absence (b) and presence (a) of pyrene. It is clearly seen that the fluorescence signal of TX-100 increases with its concentration at first, and then decreases with the concentration further increased, which is typical of an inner filter effect due to strong absorption of more exciting radiation for a more concentrated solution [32,33]. Besides that, comparing line a with b we can find that the fluorescence intensity of TX-100 in the presence of pyrene is lower than that in the absence of pyrene, which is the result of energy transfer between TX-100 and pyrene.

The energy transfer efficiency (E_{T}) calculated by Eq. (2) shows a linear rise with the increase of the surfactant concentration (Fig. 3B), and the highest value is obtained when the surfactant concentration reaches 0.43 mmol/L, and from there onward, the efficiency value decreases with the concentration of TX-100 in an exponential fashion. With the increase of the surfactant concentration, more micelles may form spontaneously and hence, more pyrene molecules are incorporated into TX-100 micelles, so the value of r decreases resulting in a sharp increase of E_{T}. However, more and more micelles are formed with the concentration of TX-100 further

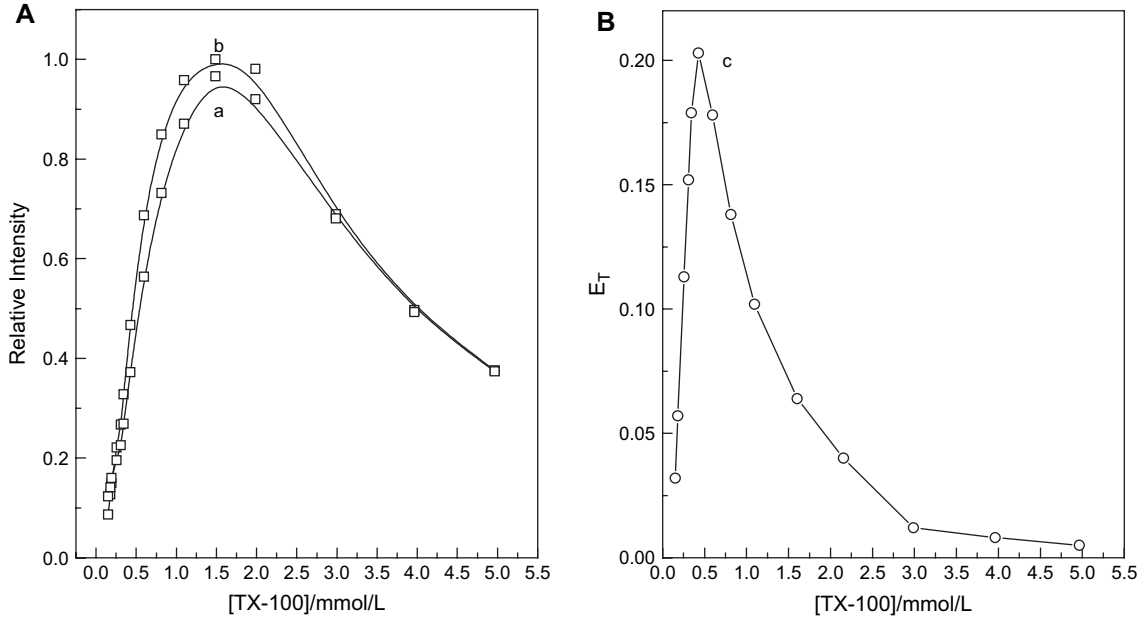

Fig. 3. Normalized fluorescence intensity of TX-100 in the presence (a) and absence (b) of pyrene (A), and the energy transfer efficiency (E_{T}) between TX-100 and pyrene (B) as a function of TX-100 concentration.

increased, so the ratio of micelles incorporated with pyrene molecules to the total micelle decreases because the concentration of pyrene is limited [33]. Besides, the inner filter effect, which is a competition process with fluorescence resonance energy transfer, is enhanced with increasing amount of TX-100 micelles in solution. So we can conclude that micelle formation facilitates energy transfer between TX-100 and pyrene, but the inner filter effect of TX-100 micelles may be the dominant process when the concentration of surfactant reaches a certain value. According to Förster theory, we can safely assume that the value of r is smallest when the E_T reaches highest. For TX-100/pyrene pairs, J of TX-100 emission and pyrene absorption spectrum is calculated, and the value is in the order of 10^{-13} M^{-1} cm^3, which agrees with Ref. [28]. And the smallest value of r calculated is 66.8 Å.

3.2. Energy transfer in TX-100/PEG$_{(aq)}$ system

The energy transfer efficiency curves obtained by adding PEG400 and PEG20000, respectively, to TX-100/pyrene aqueous solution, containing micelles, are shown in Fig. 4. The efficiency decreases sharply with PEG concentration until a relative constant value is reached. The decrease of E_T can be attributed to the enlargement of micelle size, and it has relevance to the size of micelle. So the aggregation behavior of TX-100 influenced by PEGs is investigated firstly by measurement of critical micelle concentration (cmc) and aggregate number. The determination of cmc by isothermal titration calorimetry is described in Ref. [35]. The first-order derivative of the curve of enthalpy versus surfactant concentration displays

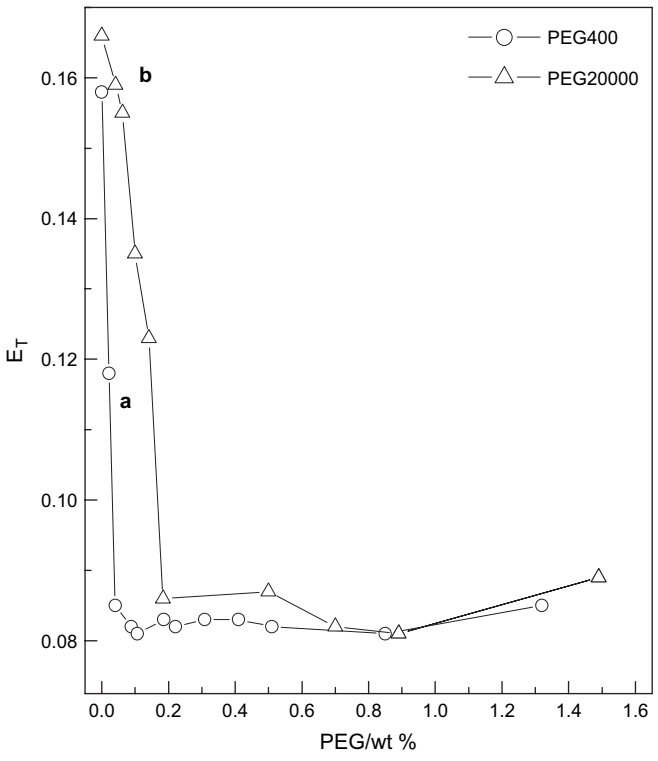

Fig. 4. Energy transfer efficiency (E_T) in TX-100/PEG$_{(aq)}$ system as a function of PEG concentration, [TX-100] = 0.40 mmol/L.

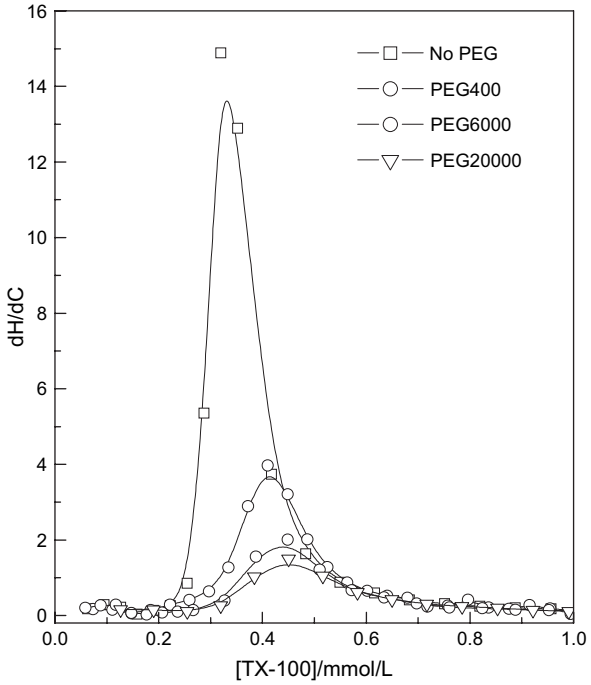

Fig. 5. The first-order derivative of the curve of enthalpy versus TX-100 concentration. [PEG] = 5 wt%.

an extremum (Fig. 5) which corresponds to cmc. The cmc value of TX-100 in the presence of 5 wt% PEG is about 0.41 mM which is almost identical to that of the pure surfactant (0.33 mM), and it is in agreement with the observation of previous studies on a different nonionic polymer and nonionic surfactant [36,37]. And the aggregate number of TX-100 in the presence of PEG is measured and listed in Table 1. From Table 1 we can see that PEGs do not change the aggregate number of TX-100. So we can safely conclude that the aggregation behavior of TX-100 is not influenced by the addition of PEG. This confirms that some of the PEG segments penetrate into TX-100 micelles resulting in the structure looseness of the aggregates is the main factor for the microstructure change of TX-100 micelles. So the average distance between phenyl rings of TX-100 and pyrene solubilized in TX-100 micelle is enlarged, and E_T between them is reduced. As the number of micelles determined by surfactant concentration is kept constant, the number of PEG segments penetrating into TX-100 micelles may reach a maximum. So from there on, the inner structure change of the complex becomes independent of PEG concentration, i.e. the interaction between TX-100 micelle and PEG is saturated. Comparing curves a and b in Fig. 4, smaller saturated concentration of PEG400 is found,

Table 1
Micellar aggregation number (N) of TX-100 and the microenvironment of pyrene (I_1/I_3) in the systems of TX-100/PEG with different molecular weight[a]

M_{PEG}	H_2O	400	1000	2000	6000	10,000	20,000
N	35.8	37.4	38.2	37.5	37.7	37.0	38.4
I_1/I_3	1.381	1.429	1.431	1.428	1.431	1.432	1.443

[a] [TX-100] = 0.7 mmol/L; [PEG] = 5 wt%.

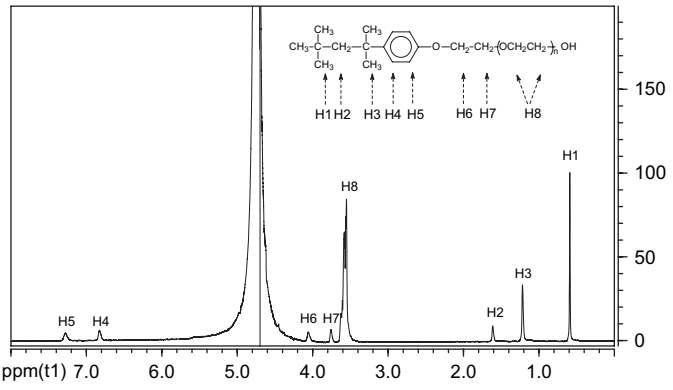

Fig. 6. ^{1}H NMR spectrum of TX-100 in water, [TX-100] = 0.70 mmol/L.

which is an evidence that shorter chain of the polymer is more efficient for structure change. The reason is that even the weight percents of the aqueous solution of PEGs with different MW are the same, the $PEG_{(aq)}$ with lower MW contains more amount of polymer chains, and hence more amount of hydrogen bonds which are at the end of the chain and easy to penetrate into micelles.

^{1}H NMR technology is used to determine whether or not the polymer chains thread through the hydrophobic core of TX-100 micelles and form ''string of beads'' complex. The ^{1}H NMR spectrum of TX-100 and the effect of PEGs with different MW on the ^{1}H chemical shifts of TX-100 are given in Fig. 6 and Table 2, respectively. PEG is a kind of linear polymer composed of repeated EO units, and threading through the hydrophobic core of TX-100 micelles possibly will change the microenvironment of the protons there, because the polarity of PEG molecular is much stronger than the alkyl chain of TX-100 molecule, and this may result in a chemical shift of protons of TX-100 hydrophobic moiety in ^{1}H NMR spectrum. However, from Table 2 we can find that the chemical shifts of the protons of alkyl chains (H1 and H3) only undergo negligible downfield shifts with the addition of PEGs, which indicate that PEG chains do not thread through the micelle cores of TX-100. However, the protons H4, H5 and H6 close to the phenoxy group exhibit significant chemical shifts. This indicates that the hydrophilic segments of PEG penetrated into the hydrophilic groups of TX-100 micelles make the amount of water combined by hydrogen bond inside the micelle increases and deteriorates the shield of protons of H4–H6. For the solution of TX-100 micelles, negligible downfield shifts

Table 2
Chemical shift variations (Δδ H) of protons of TX-100 molecule in the system of TX-100/5 wt% PEG with different molecular weight[a]

M_{PEG}	Δδ H1	Δδ H3	Δδ H2	Δδ H4	Δδ H5	Δδ H6
400	0.008	0.014	0.021	0.023	0.034	0.024
2000	0.010	0.016	0.025	0.025	0.042	0.030
6000	0.009	0.015	0.022	0.023	0.041	0.030
10,000	0.006	0.013	0.022	0.023	0.040	0.027
20,000	0.009	0.016	0.023	0.023	0.042	0.027
20,000	0.010	0.007	0.023	−0.002	−0.007	−0.002

[a] The concentration of TX-100 is 0.1 mmol/L for the last row and 0.7 mmol/L for the others.

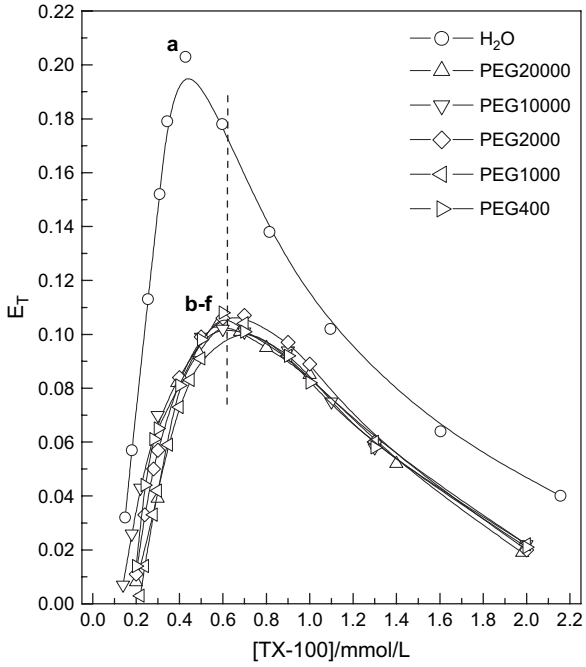

Fig. 7. Energy transfer efficiency (E_T) versus the concentration of TX-100 in the systems of TX-100/5 wt% $PEG_{(aq)}$ with different molecular weight.

of H1 and H3 can be attributed to the adsorption of TX-100 moieties on PEG chains. Because as shown in the last row of Table 2, the same extent of chemical shift is observed in dilute TX-100 aqueous solution with concentration lower than cmc.

To study the effect of the MW of PEG on the microstructure of PEG-bond aggregates of TX-100, the concentration of PEG is kept at 5 wt% to make sure that the interaction between PEG and TX-100 is saturated. Fig. 7 shows that the addition of PEG makes E_T decrease, which is independent of the MW of PEG, and the highest value of E_T still exists in the systems of TX-100/PEG, but the concentration of TX-100 corresponding to the highest E_T shifts from 0.43 mmol/L to 0.70 mmol/L. From the above discussion, we have known that the decrease of E_T with the addition of PEG is attributed to the penetration of polymer segments into TX-100 micelles and hence the enlargement of micelle size. Table 3 lists all the energy transfer parameters calculated in TX-100/$PEG_{(aq)}$ system relevant to the MW of PEG. The average distance between donor and acceptor increases from 72.5 Å to about 82 Å with

Table 3
Energy transfer parameters in TX-100/$PEG_{(aq)}$ system[a]

M_{PEG}	Φ_D	N	$J \times 10^{13}$	R_0/Å	E_T	r/Å
No PEG	0.281	1.33	7.06	58	0.162	72.5
400	0.269	1.34	6.86	56	0.109	79.0
1000	0.271	1.34	7.06	57	0.105	81.7
2000	0.270	1.34	7.19	57	0.105	81.8
6000	0.270	1.34	7.06	57	0.099	82.5
10,000	0.270	1.34	6.99	57	0.104	81.7
20,000	0.272	1.34	7.27	57	0.104	82.3

[a] [TX-100] = 0.7 mmol/L; [PEG] = 5 wt%.

the addition of PEG. So we can safely deduce that the average radius of PEG-bond aggregates is 1.13 times larger than the free micelles.

However, another factor may contribute to the donor–acceptor separation besides the enlargement of micelle size: the addition of PEGs brings about the variation of the microenvironment of the micelles, from pure water to aqueous polymer solution since the polymer segments are less hydrophilic than water as described by Qiao and Easteal [13] and will drive the solubilized pyrene to move to the outer side of TX-100 micelles. The ratio of the relative fluorescence intensity of the first (I_1) to that of the third (I_3) vibration peak of pyrene is often used to probe its microenvironment polarity. And the I_1/I_3 value rises corresponding to the increase of the polarity of the microenvironment. For pyrene solubilized in TX-100 micelles, the movement of pyrene toward the polar hydrophilic layer of TX-100 micelles can be verified by the increase of the value of I_1/I_3 caused by the addition of PEG (Table 1). So we can conclude that the size of PEG-bond TX-100 aggregate is less than 1.13 times larger than that of free micelle. And the microstructure change of TX-100 aggregates is independent of the MW of PEG, which can be verified by the effect of the MW of PEG on the microenvironment polarity of pyrene (Table 1) and chemical shift of protons of TX-100 (Table 2).

The cloud point study by Qiao and Easteal [13] shows two different interaction models between PEG and TX-100, and they propose that the structure of TX-100/PEG complex should be different from free micelles of surfactant. In the present study, the DLS experiments are done to shed light on the formation and size of PEG/TX-100 complex influenced by the MW of the polymer. Fig. 8 shows the intensity-weighted hydrodynamic radius distributions for TX-100/PEG with different molecular weights. Unimodal diffusion is observed for pure TX-100 solution and the average hydrodynamic radius $\langle R_h \rangle$ locates at about 4.80 nm which is in agreement with the value reported by Mya et al. [36]. But when PEG is added to the TX-100 solution, the DLS

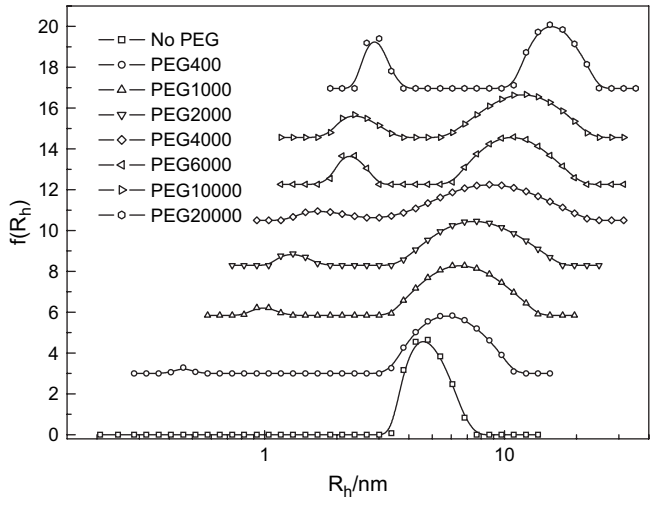

Fig. 8. Normalized hydrodynamic radius (R_h) distributions of TX-100/5 wt% PEG with different molecular weight, [TX-100] = 12 mmol/L.

Table 4
The hydrodynamic radius $\langle R_h \rangle$ of $PEG_{(aq)}$ and the system of TX-100/$PEG_{(aq)}$ with different molecular weight[a]

M_{PEG}	$PEG_{(aq)}$[b]	TX-100/PEG	
	R_h/nm	R_h/nm (fast)	R_h/nm (slow)
No PEG	–	–	4.80
400	0.42	0.46	5.90
1000	0.65	0.99	6.69
2000	0.91	1.32	7.65
4000	1.29	1.57	8.44
6000	1.58	2.27	10.95
10,000	2.00	2.43	11.76
20,000	2.90	2.90	16.06

[a] [TX-100] = 12 mmol/L; [PEG] = 5 wt%.
[b] The values are calculated by equations in Ref. [38].

correlation functions become bimodal, i.e. the initial narrow peak splits into two peaks corresponding to fast and slow modal, respectively. The $\langle R_h \rangle$ value of the fast modal in the presence of PEG is much more less than that of TX-100 micelles, and almost the same with the size of isolated PEG coil and increases with the MW of PEG (Table 4). This result suggests that the fast modal corresponds to isolated PEG coil [38]. The $\langle R_h \rangle$ of slow modal in the presence of PEG is larger than that of free TX-100 micelles (Table 4), which indicates the formation of TX-100/PEG complex by the penetration of PEG into TX-100 micelle and is in accordance with the result of the FRET (Table 3). In addition, the $\langle R_h \rangle$ value of the slow modal increases with the MW of PEG, and it is even more than two times of free micelles for the system of TX-100/PEG with higher MW of PEG, which indicates the formation of multimicellar complex. Taking the system of TX-100/PEG20000 for an example, the polymer has about 454 CH_2–CH_2–O monomers and the chain contour length is about 82 nm (monomer length about 0.18 nm) [39], but the circumference of free TX-100 micelle is only about 30 nm (radius about 4.8 nm). Thus, we can assume that the chain of PEG20000 can wrap effectively about the surface of approximately three micelles, resulting that the $\langle R_h \rangle$ of complex is three times of free micelles (Table 4).

The configuration of TX-100/PEG complex is demonstrated in Fig. 9 using freeze-fractured transmission microscopy. For PEGs with MW less than 2000 Da, most of the complexes of TX-100/PEG take on sphere structure and distribute uniformly in solution (Fig. 9B and C) just as the free TX-100 micelles (Fig. 9A). However, when MW is larger than 2000 Da, PEG chains interact with more than one TX-100 aggregates simultaneously, making micelles get close to each other and forming coral-shaped clusters (Fig. 9D–G). This is in accordance with the results of DLS shown in Fig. 8. The results of FRET and ^{1}H NMR show that some segments of the polymer chain penetrate into the hydrophilic groups of TX-100 aggregates or absorb on the surface of micelles, and the others remain in bulk solution forming strong hydrogen bond with water. The interaction models of the complex of TX-100/PEG are shown in Fig. 10. It should be noted that the concepts of lower molecular weight and the higher molecular weight PEGs are relative to the size of the micelles

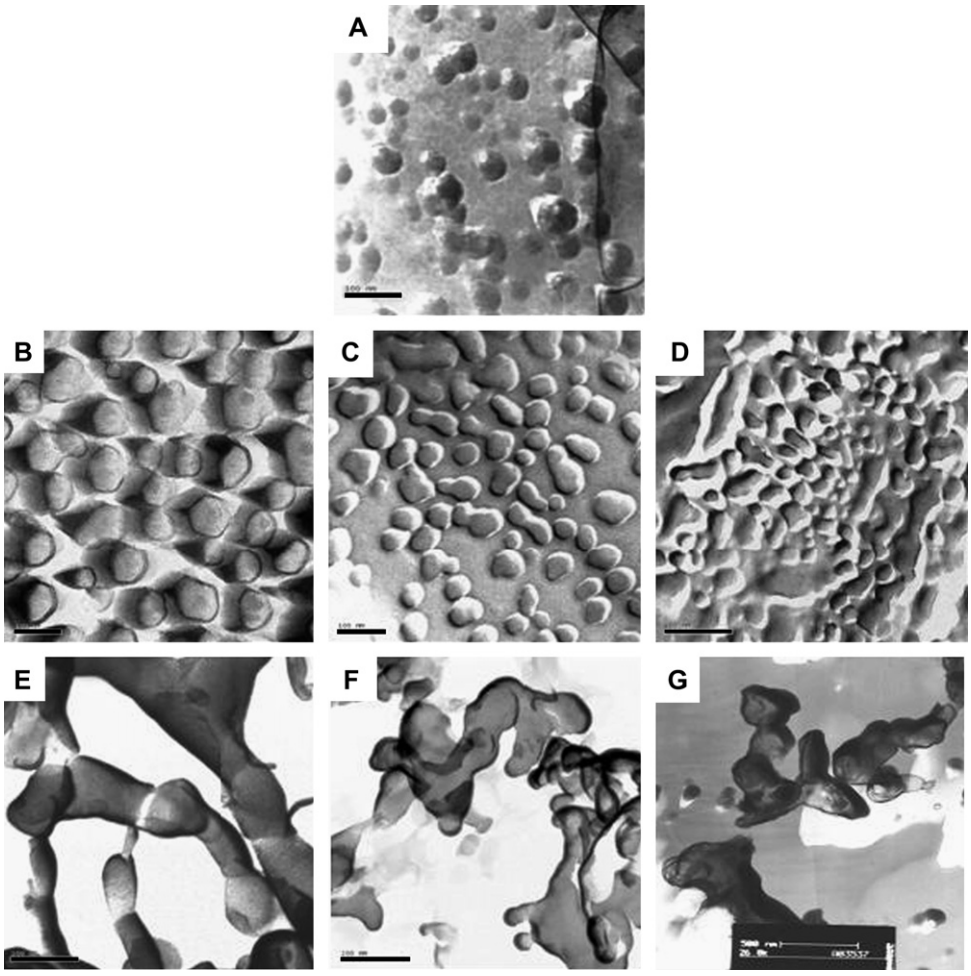

Fig. 9. FF-TEM of the system of TX-100/0.8 wt% $PEG_{(aq)}$ with polymer molecular weight: (A) no PEG, (B) 400, (C) 1000, (D) 2000, (E) 4000, (F) 6000, and (G) 10,000. [TX-100] = 12 mmol/L. Scale bars: (A–D): 100 nm, (E–F): 200 nm, (G): 500 nm.

with which they will interact. In TX-100/$PEG2000_{(aq)}$ solution, two kinds of configuration are both observed, which indicates that 2000 Da is the critical MW of PEG for TX-100 micelles which are in good agreement with cloud point studies in the literature [13]. In addition, the size of the aggregates measured by FF-TEM is larger than the result of DLS because the frozen samples gilded with platinum make the replica much larger, but the morphology and relative size inflected by FF-TEM are in agreement with the result of DLS.

3.3. Effect of temperature on energy transfer

To explore the effect of temperature on the energy transfer, we pay attention to the systems in the presence of PEG400 and PEG20000, respectively, which are the highest and lowest MW of the polymer studied. The concentration of PEG is fixed at 5 wt% and that of surfactant changes. The value of E_T decreases when the temperature rises from 25 °C to 50 °C (Fig. 11) and this can be ascribed to thermal quenching which

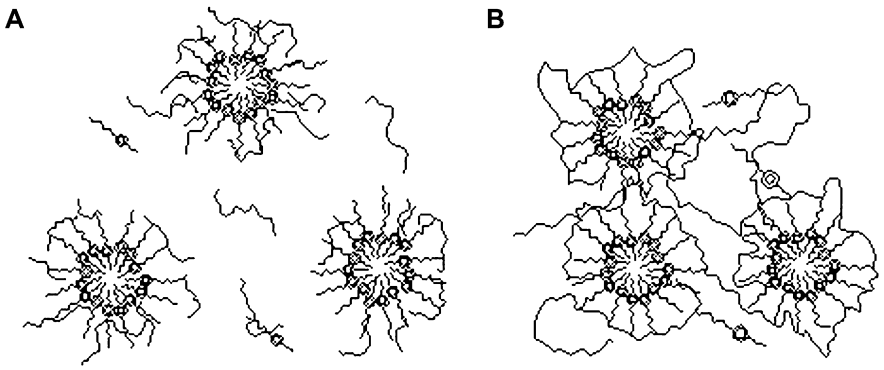

Fig. 10. Illustration of TX-100/PEG complex with lower PEG molecular weight (MW < 2000 Da) (A) and higher PEG molecular weight (MW > 2000 Da) (B).

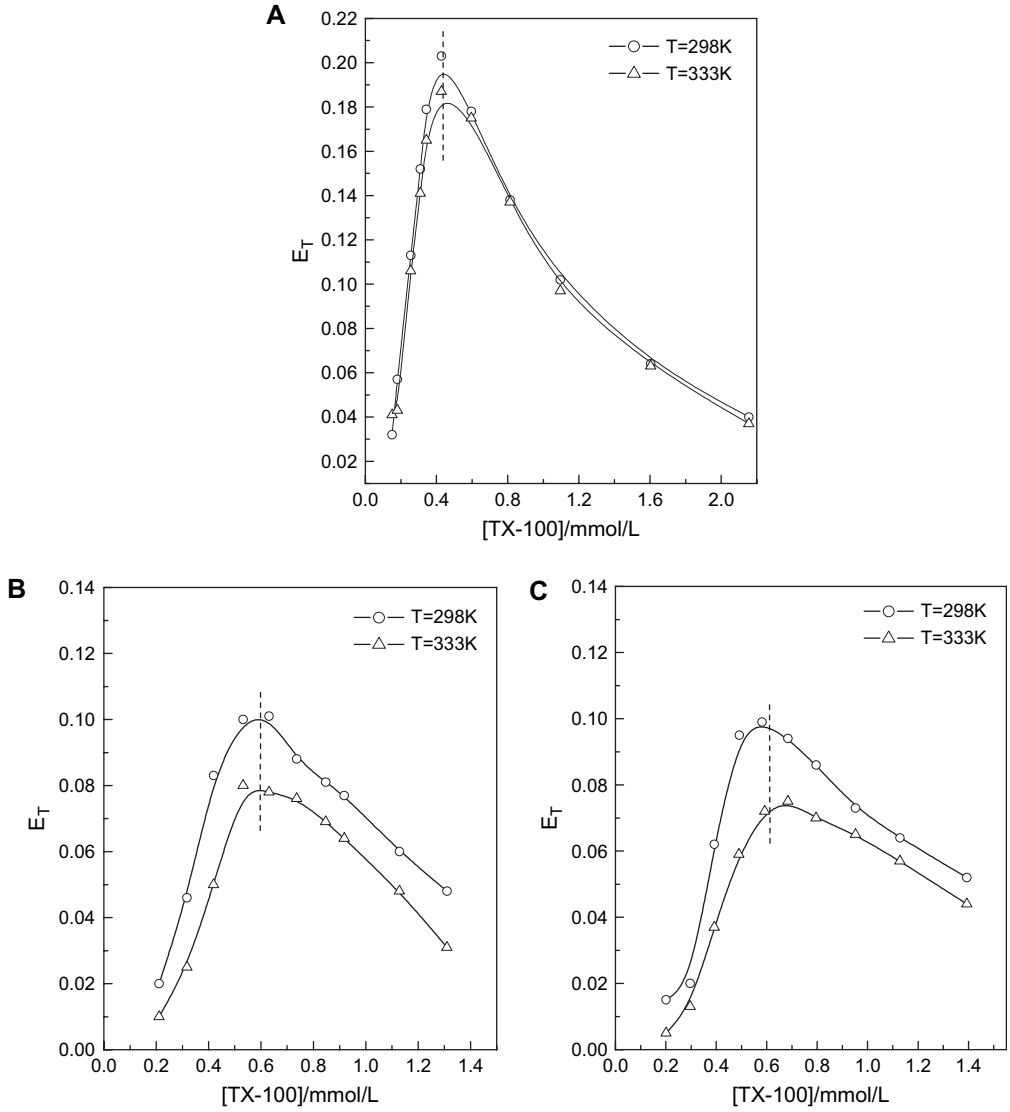

Fig. 11. Energy transfer efficiency (E_T) in the systems of (A) TX-100 aqueous solution, (B) TX-100/5 wt% PEG400$_{(aq)}$, and (C) TX-100/5 wt% PEG20000$_{(aq)}$ at 298 K (○) and 333 K (Δ).

is a competition process with energy transfer, i.e. the moving rate of particles in solution rises with increasing temperature, and hence, more of the excited TX-100 monomers and aggregates lose their energy through collision with each other. And the size of TX-100 micelles may get larger with the increase of aggregation number as reported in previous studies [32], causing the separation of donor and acceptor.

An interesting feature of Fig. 11 is that the reduction of E_T with temperature is much more obvious for the systems in the presence of PEGs than in the absence of them. The maximum value of E_T and the corresponding value of r of all the three systems at 25 °C and 50 °C, respectively, are calculated and listed in Table 5. For the three systems concerned, the value of r increases by 1.1 Å for TX-100/pyrene$_{(aq)}$, and 4 Å or so for TX-100/PEG$_{(aq)}$ when the temperature rises from 25 °C to 50 °C, which is an evidence that more segments of the polymer penetrate into the surfactant aggregates with increasing temperature, resulting in enlargement of TX-100 micelle and hence the increased value of r. This suggests that the interaction between polymer and surfactant aggregate has been enhanced with rising temperature as the dehydration of EO chains of TX-100 is enhanced with rising temperature and more hydrophilic moieties of TX-100 molecules are relaxed and interact with PEG chains. In addition, the effect of

Table 5
Energy transfer efficiency (E_T) and donor–acceptor separation (r) in TX-100/PEG$_{(aq)}$ system at 298 K and 333 K[a]

Solution	T/K	E_T	r/Å
No PEG	298	0.203	66.8
	333	0.187	67.9
PEG400	298	0.101	80.1
	333	0.078	84.0
PEG20000	298	0.099	83.1
	333	0.075	87.4

[a] [TX-100] = 0.7 mmol/L; [PEG] = 5 wt%.

temperature on TX-100–PEG interaction is independent of the polymer chain length because the segment penetrating into micelles, which is determined mainly by polymer concentration, reaches saturation.

3.4. Effect of alcohol on energy transfer

Aliphatic alcohols with different chain lengths, often used as co-surfactants, can change the structure and stability of surfactant aggregates. Here the fluorescence resonance energy transfer is used to explore the effect of unbranched aliphatic alcohols on the microstructure of TX-100/PEG complex. The effects of alcohols with different carbon numbers ranging from 3 to 6 on the E_T of TX-100/pyrene in the presence and absence of PEG are shown in Fig. 12. From Fig. 12 we can see that propanol has negligible effect on E_T for its higher hydrophilicity, and the others with longer chains reduce the value of E_T. This is in accordance with the result that the alcohols with longer hydrocarbon chain are relatively more easily solubilized in the micelle phase [40,41], enlarging the micelle size and driving the hydrophobic pyrene into the inside of the micelle core, increasing the average distance r, so the value of E_T decreases.

Since the alcohols with carbon numbers of 4–6 have almost the same effect on E_T, n-$C_5H_{11}OH$ is chosen for further investigation. Fig. 13 shows the effect of the concentration of n-$C_5H_{11}OH$ on E_T of TX-100/pyrene system in the presence and absence of PEG. From the discussion in Section 3.2 we have known that the reduction of E_T with the addition of PEG is mainly due to the complex formation of TX-100/PEG.

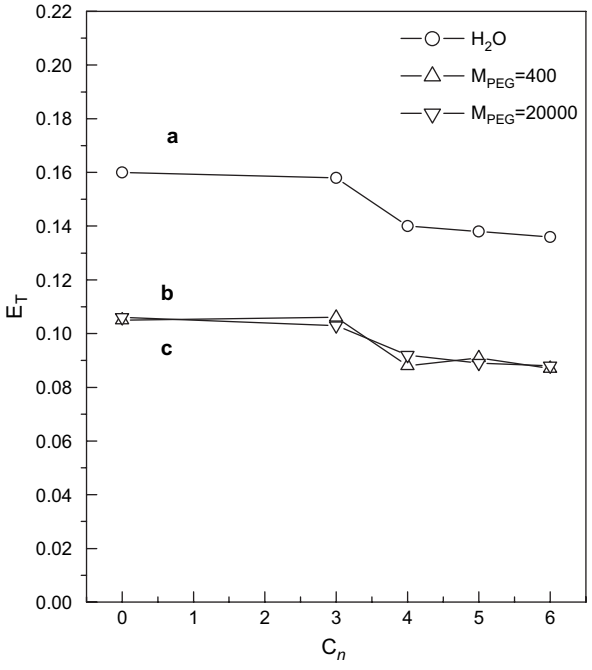

Fig. 12. The effects of normal alcohol carbon numbers (C_n) on the energy transfer efficiency (E_T) in the systems of (a) TX-100 aqueous solution, (b) TX-100/PEG400$_{(aq)}$, and (c) TX-100/PEG20000$_{(aq)}$, [PEG] = 5 wt%, [n-$C_nH_{2n+1}OH$] = 0.32 wt%, [TX-100] = 0.7 mmol/L.

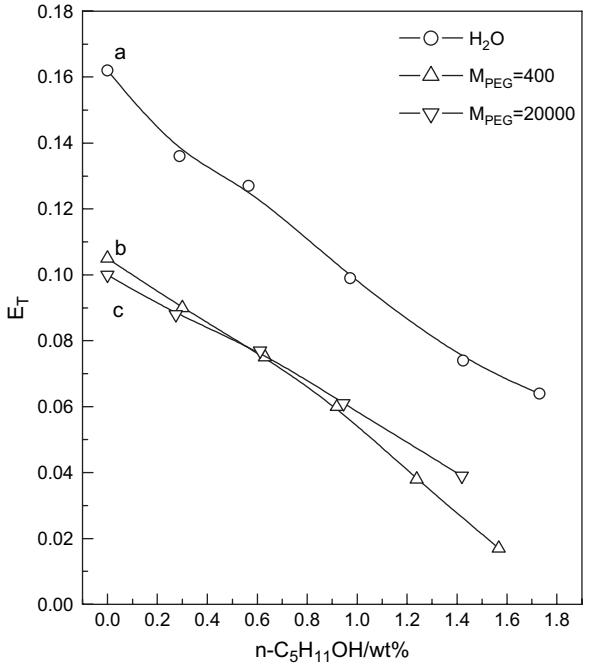

Fig. 13. The energy transfer efficiency (E_T) from TX-100 to pyrene in the absence (a) and presence of PEG400 (b) and PEG20000 (c) as a function of n-$C_5H_{11}OH$ concentration, [TX-100] = 0.7 mmol/L, [PEG] = 5 wt%.

However, for the system that contains alcohols, PEG may change the distribution ratio of alcohol in micelle phase and water phase, which would possibly change its effect on micelle size and affect the energy transfer efficiency. So the effect of PEG on the distribution coefficients (K_x) of n-$C_5H_{11}OH$ in micelle phase, together with the transfer Gibbs free energy (ΔG_t) from water phase to micelle phase, is measured using the method mentioned in the literature [42] and listed in Table 6. From Table 6 we can find that $\Delta G_t < 0$, which is in accordance with the literature [34], indicating that the transfer of pentanol from water to micelle phase is spontaneous. The slight decrease of K_x and the increase of ΔG_t, suggest that PEG with higher MW may hinder the solubilization of alcohol in micelle phase, i.e. the higher MW of PEG, the less amount of alcohol may locate in micelle phase, and hence the slighter size change of surfactant aggregates with the addition of alcohol. However, comparing lines b and c, we can find that the energy transfer efficiency is almost independent of MW of PEG, which indicates that the effect of TX-100/PEG complex formation is dominant in structure change of the surfactant aggregates, and this is in agreement with the discussion in the above paragraph.

Table 6
Distribution coefficients (K_x) and the transfer Gibbs energy (ΔG_t) of n-$C_5H_{11}OH$ in TX-100/PEG$_{(aq)}$ system[a]

M_{PEG}	No PEG	400	4000	10,000
K_x	228.5	220.0	182.4	168.6
ΔG_t/(kJ/mol)	−13.46	−13.36	−12.90	−12.70

[a] [TX-100] = 0.7 mmol/L; [PEG] = 5 wt%.

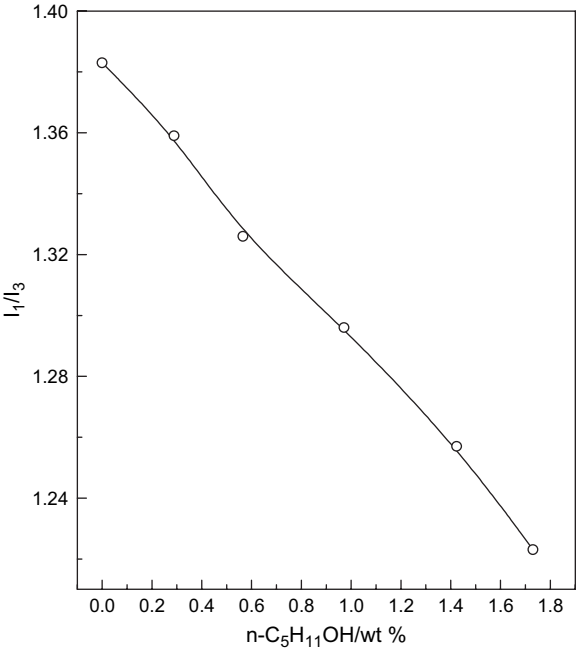

Fig. 14. The microenvironment of pyrene (I_1/I_3) in TX-100/*n*-$C_5H_{11}OH$ system versus the concentration of *n*-$C_5H_{11}OH$, [TX-100] = 0.7 mmol/L.

On the basis of Fig. 13, in which the decreased value of E_T as a result of PEG addition is independent of alcohol concentration (comparing lines b and c with line a), we can conclude that alcohols do not affect TX-100/PEG complex formation. On the other hand, the decreasing trend of E_T within all the alcohol concentrations studied is almost the same no matter with or without PEG, which indicates that the addition of PEG does not affect the solubilization of alcohols in surfactant aggregates, i.e. the formation of TX-100/PEG complex does not hinder the solubilization behavior of micelles. In addition, the decrease of E_T with the rising alcohol concentration can be attributed to the increasing amount of alcohol molecules located in the micelle phase and results in the inward movement of pyrene in TX-100 micelles, which can be verified by the polarity dropping as shown in Fig. 14.

4. Conclusion

PEG does not thread through TX-100 micelles but is absorbed on the surface or penetrate into the hydrophilic layer of TX-100 micelles and forms TX-100/PEG complex with two configurations: the sphere-like structure for shorter chains of PEG (MW < 2000) and the coral-like clusters for longer chains of PEG (MW > 2000). The formation of TX-100/PEG complex enlarges the micelle size, which is independent of the MW of PEG when their interaction is saturated, i.e. the microstructure of PEG-bond aggregates of TX-100, no matter with sphere-like or coral-like configurations, is the same. In addition, rising temperature facilitates the formation of complex, while alcohols do not affect the formation.

Acknowledgement

This work was supported by the National Nature Science Foundation of China (no. 20633010).

References

[1] Mészáros R, Varga I, Gilányi T. J Phys Chem B 2005;109:13538–44.
[2] Middleton H, English RJ, Williams PA. Langmuir 2005;21:5174–8.
[3] Deo P, Deo N, Somasudaran P. Langmuir 2005;21:9998–10003.
[4] (a) Guo XH, Abdala AA, May BL, Lincoln SF, Khan SA, Prud'homme RK. Polymer 2006;47:2976–83;
(b) Bai SL, Wang GT, Hiver JM, G'Sell C. Polymer 2004;45:3063–71.
[5] Holland NB, Xu Z, Vacheethasanee K, Marchant RE. Macromolecules 2001;34:6424–30.
[6] Razatos A, Ong YL, Boulay F, Elbert DL, Hubbell JA, Sharma MM. Langmuir 2000;16:9155–8.
[7] Holownina P, Amodio SP, Price CP. Anal Chem 2001;73:3426–31.
[8] Nisha CK, Manorama SV, Kizhakkedathu JN, Maiti S. Langmuir 2004;20:8468–75.
[9] Nolan CM, Reyes CD, Debord JD, García AJ, Lyon LA. Biomacromolecules 2005;6:2032–9.
[10] Deo P, Somasundaran P. Langmuir 2005;21:3950–6.
[11] Nakano SI, Karimata H, Ohmichi I, Kawakami J, Sugimoto N. J Am Chem Soc 2004;126:14330–1.
[12] Borisov OV, Halperin A. Macromolecules 1996;29:2612–7.
[13] Qiao L, Easteal A. J Colloid Polym Sci 1998;276:313–20.
[14] Schild HG, Tirrell DA. Macromolecules 1992;25:4553–8.
[15] Kujawa P, Liu R, Winnik F. Phys Chem B 2002;106:5578–85.
[16] Jons CD, McGrath JG, Lyon LA. J Phys Chem B 2004;108:12652–7.
[17] Itaka K, Harada A, Nakamura K, Kawaguchi H, Kataoka K. Biomacromolecules 2002;3:841–5.
[18] Oh JK, Yang J, Tomba JP, Rademacher J, Farwaha R, Winnik MA. Macromolecules 2003;36:8836–45.
[19] Laukkanen A, Winnik FM, Tenhu H. Macromolecules 2005;38:2439–48.
[20] Schenning APHJ, Peters E, Meijer EW. J Am Chem Soc 2000;122:4489–95.
[21] Jayachandran KN, Maiti S, Chatterji PR. Polymer 2001;42:6113–8.
[22] Ye XD, Farinha JPS, Oh JK, Winnik MA, Wu C. Macromolecules 2003;36:8749–60.
[23] Zhang GX. Principles of surfactant action. Beijing: Chinese Light Industry Press; 2003. p. 38.
[24] Li LD, Zhang M. Chin J Anal Chem 1988;16:732–4.
[25] Berne BJ, Pecora R. Dynamic light scattering. New York: Plenum Press; 1976.
[26] Guo R, Liu TQ, Yu WL. Langmuir 1999;15:624–30.
[27] Förster TO, Sinanoglu, editors. Modern quantum chemistry, vol. 3. New York: Academic Press; 1966. p. 93.
[28] De S, Girigoswami A. J Colloid Interface Sci 2004;271:485–95.
[29] Tamura H, Knoche M, Bukovac M. J Agric Food Chem 2001;49:1809–16.
[30] Saha DC, Ray K, Misra TN. Spectrochim Acta Part A 2000;56:797–801.
[31] Kikuchi K, Takakusa H, Nagano T. Trends Anal Chem 2004;23:407–15.
[32] Guo R, Ding YH, Liu TQ. Acta Chim Sin 1999;57:943–52.
[33] Fanget B, Devos O. Anal Chem 2003;75:2790–5.
[34] Toerne K, Wandruszka RV. Langmuir 2002;18:7349–53.
[35] Dai S, Tam KC. Langmuir 2004;20:2177–83.
[36] Mya KY, Jamieson AM, Sirivat A. Polymer 1999;40:5741–9.
[37] Brckman JC, van Os NM, Engberts JBFN. Langmuir 1988;4:1266–9.
[38] López-Esparza R, Gurdeau-Boudeville M-A, Cambin Y, Rodríguez-Beas C, Maldonado A, Urbach W. J Colloid Interface Sci 2006;300:105–10.
[39] Feitosa E, Brown W, Wang K, Barreleiro PCA. Macromolecules 2002;35:201–7.
[40] Kumar P, Mittal KL. Handbook of microemulsion science and technology; 1999. p. 139–84.
[41] Guo R, Ding YH, Liu TQ. J Dispersion Sci Technol 2002;23:777–88.
[42] Tokuoka Y, Uchiyama H, Abe M. Langmuir 1995;11:725–9.